PHYSICS OF FLUIDS **27**, 105104 (2015)

A minimal model of self-sustaining turbulence

Vaughan L. Thomas,[1] Brian F. Farrell,[2] Petros J. Ioannou,[3] and Dennice F. Gayme[1]
[1]*Department of Mechanical Engineering, Johns Hopkins University, Baltimore, Maryland 21218, USA*
[2]*School of Engineering and Applied Sciences, Harvard University, Cambridge, Massachusetts 02138, USA*
[3]*Department of Physics, National and Kapodistrian University of Athens, Panepistimiopolis, Zografos, Athens 15784, Greece*

(Received 6 January 2015; accepted 14 September 2015; published online 8 October 2015)

In this work, we examine the turbulence maintained in a Restricted Nonlinear (RNL) model of plane Couette flow. This model is a computationally efficient approximation of the second order statistical state dynamics obtained by partitioning the flow into a streamwise averaged mean flow and perturbations about that mean, a closure referred to herein as the RNL_∞ model. The RNL model investigated here employs a single member of the infinite ensemble that comprises the covariance of the RNL_∞ dynamics. The RNL system has previously been shown to support self-sustaining turbulence with a mean flow and structural features that are consistent with direct numerical simulations (DNS). Regardless of the number of streamwise Fourier components used in the simulation, the RNL system's self-sustaining turbulent state is supported by a small number of streamwise varying modes. Remarkably, further truncation of the RNL system's support to as few as one streamwise varying mode can suffice to sustain the turbulent state. The close correspondence between RNL simulations and DNS that has been previously demonstrated along with the results presented here suggest that the fundamental mechanisms underlying wall-turbulence can be analyzed using these highly simplified RNL systems. © *2015 AIP Publishing LLC.* [http://dx.doi.org/10.1063/1.4931776]

I. INTRODUCTION

The analytical intractability of the Navier Stokes (NS) equations has impeded attempts to develop a comprehensive understanding of the dynamics of turbulence in wall-bounded shear flows. This impediment to understanding resulting from the complexity of NS dynamics has led to extensive efforts to obtain simplifications of the NS system that still retain fundamental aspects of the dynamics of wall-turbulence. One useful approach for simplifying the NS system is to study models of reduced order. Model order reduction can be accomplished by Galerkin projections of the infinite dimensional NS system onto a finite low dimensional space. The basis functions used are generally chosen for their particular properties, such as Fourier modes for use in Cartesian channels with diffusive dissipation, Proper Orthogonal Decomposition (POD) projections[1,2] for economy in representing the structures occurring in turbulence, and balanced truncation for economical representations of turbulence dynamics.[3–5]

A second area of research aimed at understanding the dynamics underlying the NS equations is the study of systems in which the complexity of the dynamics has been reduced. One such method is confining the turbulence to a minimal channel that reduces the complexity of supported perturbations and results in a simplification of the flow structures. This method was used to demonstrate the importance of large-scale roll and streak structures in maintaining turbulence. In particular, a minimal channel was used to show that wall-turbulence does not self-sustain unless the confining channel is large enough to accommodate roll and streak structures of sufficient spanwise and streamwise extents.[6,7]

Reduction of the support of turbulence has also been attempted by seeking a skeleton of exact coherent structures in the phase space of the transient turbulent attractor, see, e.g., Refs. 8 and 9. For plane Couette flow, the first such unstable solution was the fixed point computed by Nagata.[10] Subsequent research using numerical methods has uncovered additional fixed points and periodic orbits for plane Couette flow.[9,11] While promising conceptually, the project of extending these solutions to the global turbulent dynamics has yet to be completed. A related approach is to isolate and model specific flow features and interactions in a schematic fashion, examples of this approach include the roll/streak instability self-sustaining process (SSP) model,[7] the nine-mode truncation model of Moehlis *et al*.,[12] and the model describing laminar-turbulent spots and structures by Tuckerman and Barkley.[13]

Another method of reducing the complexity of turbulence dynamics is to simplify the equations themselves. One example of this approach is to study turbulence using the Linearized Navier Stokes (LNS) equations, which can be analyzed comprehensively using linear systems theory.[14,15] The LNS equations capture a number of fundamental aspects of turbulence dynamics including the non-normal disturbance amplification mechanism,[16–23] which has been shown to be necessary for energy production in fully turbulent flow[24] and to play a key role in the bypass transition mechanism.[25] The LNS equations also provide specific insights into the mechanism maintaining turbulence including the role of the coupling between the Orr-Sommerfeld and Squire equations in generating the robust transient growth of streaks by the lift-up process that is an integral component of the roll/streak mechanism underlying the SSP in wall-bounded shear flows.[26,27] The LNS equations have also proven successful in predicting second-order statistics in these flows.[26,28–34]

The current work employs a statistical state dynamics (SSD) model that incorporates a combination of the reduction of order and the simplification of dynamics approaches. This model is based on the restricted nonlinear (RNL) dynamical system, which is a second order closure of the dynamics of the turbulent statistical state comprising the joint evolution of the streamwise constant mean flow (first cumulant) and the ensemble second order perturbation statistics (second cumulant). The SSD is closed either by parametrizing the higher cumulants using stochastic excitation or by setting the third cumulant to zero, see, e.g., Ref. 50. Restricting the NS equations to the first two cumulants retains the nonlinear interaction between the perturbation momentum fluxes and the mean flow but neglects explicit calculation of the nonlinear interactions among the streamwise varying perturbations. Turbulence was first studied in a RNL modeling framework using the stochastic structural stability theory system,[35] which we will refer to as the RNL_∞ system. In the RNL_∞ system, the second cumulant is obtained by solving the time dependent Lyapunov equation for the perturbation covariance dynamics. This time dependent Lyapunov equation represents the dynamics of an infinite ensemble of realizations of the perturbation structure. As a result, the SSD of the RNL_∞ system is autonomous, which is particularly useful for obtaining analytical results. However, the covariance matrix dimension for a perturbation dynamics of $O(N)$ is $O(N^2)$, which limits the resolution of models that can be studied directly using the RNL_∞ model. In order to overcome this limitation in subsequent implementations of the RNL model, the covariance was estimated from a single realization of the perturbation dynamics.[36,37] This approximation shares the dynamical restrictions of the RNL_∞ system but, unlike the RNL_∞ model, it retains small fluctuations in the perturbation covariance due to the perturbation covariance dynamics not being that of an infinite ensemble. It is this dynamical restriction that is primarily responsible for the insights into turbulence dynamics obtained from the RNL framework.[36,37] The existence of fluctuations in the approximate covariance does not greatly affect the correspondence between simulation results obtained using the analytically tractable RNL_∞ and those obtained with the numerically tractable RNL implementation used in this work.[36]

The goals of this work are to further investigate the dynamics of RNL turbulence and to examine the implications of its simplified structure for understanding wall-turbulence. The primary focus of our study is the mechanisms that maintain the turbulent flow and determine the structure of its statistical mean state. It is natural that in studying these mechanisms, attention is focused on the dynamics of the streak and roll structures. These structures, which are ubiquitous in wall-turbulence, respectively, comprise the large-scale streamwise streaks of high and low speed fluids and the associated streamwise vortices, the circulations of which reinforce the streaks through

the linear non-normal lift-up mechanism. Understanding the dynamical mechanisms determining the structure of the mean and perturbation fields and maintaining the statistical equilibrium state of wall-turbulence require understanding the dynamics of these structures. The rolls and streaks in wall-turbulence are not associated with an unstable linear mode but rather are maintained by a nonlinear instability process that is associated with linear non-normal growth of both the streamwise invariant roll and streak structures and the streamwise varying perturbation fields that maintain the roll structure. A dynamical mechanism advanced to explain this nonlinear instability is referred to as a SSP. The first such process traced the origin of the perturbations required to sustain linear non-normal streak growth to the break-up of previously generated streaks.[38–41] An alternative explanation of the SSP suggested that Reynolds stresses arising from inflectional instability of the streak maintain the roll circulations.[7,42,43] However, analysis of simulations subsequently revealed that most streaks are too weak to sustain strong inflectional instability, which resulted in the suggestion that transient growth gives rise to the roll-maintaining perturbations.[41] Transiently growing perturbations have also been shown to maintain the roll circulation in the RNL system. However, in contrast to previously proposed transient growth based mechanisms,[40,41] the transiently growing perturbations in RNL turbulence result not from the random occurrence of optimal perturbations associated with streak breakdown but rather from systematic parametric instability of the time-dependent streak.[15,44,45]

In this work, we study the RNL dynamics both by approximating the closure for the third cumulant of the RNL_∞ SSD using a stochastic forcing and by approximating the closure of this SSD that sets the third cumulant to zero. The main results demonstrate that RNL turbulence is naturally maintained solely through interactions between the streamwise mean flow (i.e., the $k_x = 0$ streamwise Fourier component) and a small set of streamwise varying modes (i.e., the $k_x \neq 0$ streamwise Fourier components). Moreover, we establish that a minimal configuration for maintaining turbulence can be obtained by limiting the streamwise Fourier support of the RNL turbulence to a single streamwise varying mode. A second contribution of this work is an investigation of RNL turbulence in extended channels. Specifically, we show that RNL turbulence self-sustains in channels with streamwise extents of $96\pi\delta$, where δ is the half channel height. These results suggest that self-sustaining RNL turbulence continues to exist in channels with infinite streamwise extent.

This paper is organized as follows. Section II contains a derivation of the RNL model from the NS equations and establishes its relation to the RNL_∞ system. In Section III, we describe our numerical approach. Then, in Section IV, we show that the RNL system naturally maintains a turbulent state that is consistent with that of direct numerical simulations (DNS) and that RNL turbulence is supported by only a small set of streamwise Fourier components (modes). In Section IV B, we truncate the streamwise wavenumbers over which RNL turbulence is sustained to a single streamwise varying mode and explore the set of these streamwise wavenumbers over which the turbulence is sustained. We also explore the sensitivity of the turbulence statistics to the retained wavenumber. Finally, we conclude the paper and point to directions of future study.

II. MODELING FRAMEWORK

Consider a plane Couette flow between walls with velocities $\pm U_w$. The streamwise direction is x, the wall-normal direction is y, and the spanwise direction is z. Quantities are non-dimensionalized by the channel half-width, δ, and the wall velocity, U_w. Time, t, is non-dimensionalized by δ/U_w. The lengths of the channel in the streamwise and spanwise directions are, respectively, L_x and L_z. Streamwise averaged, spanwise averaged, and time-averaged quantities are, respectively, denoted by angled brackets, $\langle \bullet \rangle = \frac{1}{L_x}\int_0^{L_x} \bullet \, \mathrm{d}x$, square brackets, $[\bullet] = \frac{1}{L_z}\int_0^{L_z} \bullet \, \mathrm{d}z$, and an overline $\overline{\bullet} = \frac{1}{T}\int_0^{T} \bullet \, \mathrm{d}t$, with T sufficiently large. The velocity field $\mathbf{u}_T$ is decomposed into a streamwise averaged mean, $\mathbf{U}(y,z,t) = (U,V,W)$, and the deviation from this mean (the perturbation), $\mathbf{u}(x,y,z,t) = (u,v,w)$. The pressure gradient is similarly decomposed into a streamwise averaged mean, $\nabla P(y,z,t)$, and the deviation from this mean, $\nabla p(x,y,z,t)$. The corresponding NS equations are

$$\mathbf{U}_t + \mathbf{U}\cdot\nabla\mathbf{U} + \nabla P - \frac{1}{R}\Delta\mathbf{U} = -\langle\mathbf{u}\cdot\nabla\mathbf{u}\rangle, \tag{1a}$$

$$\mathbf{u}_t + \mathbf{U}\cdot\nabla\mathbf{u} + \mathbf{u}\cdot\nabla\mathbf{U} + \nabla p - \frac{1}{R}\Delta\mathbf{u} = -\left(\mathbf{u}\cdot\nabla\mathbf{u} - \langle\mathbf{u}\cdot\nabla\mathbf{u}\rangle\right) + \epsilon, \tag{1b}$$

$$\nabla\cdot\mathbf{U} = 0, \quad \nabla\cdot\mathbf{u} = 0, \tag{1c}$$

where ϵ is a stochastic excitation used to initiate turbulence and the Reynolds number is defined as $R = U_w\delta/\nu$, with kinematic viscosity ν.

Obtaining the SSD corresponding to (1) requires solving the infinite hierarchy of cumulant equations, see, e.g., Refs. 46 and 47. However, a useful and tractable approximation to the full SSD is obtained by closing this infinite hierarchy at second order by either neglecting the third cumulant or parametrizing it appropriately. We refer to this approximation as the RNL_∞ system and use the ∞ to indicate that the ensemble of realizations is infinite. Physical realizations of the RNL_∞ system can be obtained by making the ergodic assumption that the ensemble averages and streamwise averages are equal and consequently, the first cumulant is the streamwise averaged flow. In this work, we will approximate the second cumulant of the RNL_∞ dynamics by the streamwise average of the spatial two-point correlations obtained from a single $\mathbf{u}$ field realization. The resulting approximation to the RNL_∞ system is governed by the following equations:

$$\mathbf{U}_t + \mathbf{U}\cdot\nabla\mathbf{U} + \nabla P - \frac{1}{R}\Delta\mathbf{U} = -\langle\mathbf{u}\cdot\nabla\mathbf{u}\rangle, \tag{2a}$$

$$\mathbf{u}_t + \mathbf{U}\cdot\nabla\mathbf{u} + \mathbf{u}\cdot\nabla\mathbf{U} + \nabla p - \frac{1}{R}\Delta\mathbf{u} = \mathbf{e}, \tag{2b}$$

$$\nabla\cdot\mathbf{U} = 0, \quad \nabla\cdot\mathbf{u} = 0. \tag{2c}$$

We refer to Equation (2) as the RNL model. The dynamics in (2) correspond to setting $\varepsilon = 0$ and parametrizing the perturbation-perturbation nonlinearity, $\mathbf{u}\cdot\nabla\mathbf{u} - \langle\mathbf{u}\cdot\nabla\mathbf{u}\rangle$ in (1b), with the stochastic excitation $\mathbf{e}$. These equations approximate the closure of the SSD at second order using a stochastic parametrization of the higher order cumulants or alternatively by neglecting the third cumulant, which corresponds to setting $\mathbf{e} = \mathbf{0}$. Nonlinear equation (2a) describes the dynamics of a streamwise averaged mean flow driven by the divergence of the streamwise averaged Reynolds stresses, which we denote by, e.g., $\langle uu\rangle$, $\langle uv\rangle$. Equation (2b) describes the influence of the streamwise constant mean flow, $\mathbf{U}(y,z,t)$, on the linearized perturbation dynamics.

III. NUMERICAL APPROACH

The numerical simulations in this paper were carried out using a spectral code based on the Channelflow NS equations solver.[48,49] The time integration uses a third order multistep semi-implicit Adams-Bashforth/backward-differentiation scheme that is detailed in Ref. 50. The discretization time step, Δt, is automatically adjusted such that the Courant-Friedrichs-Lewy (CFL) number is kept between 0.05 and 0.2. The spatial derivatives employ Chebyshev polynomials in the wall-normal (y) direction and Fourier series expansions in the streamwise (x) and spanwise (z) directions.[51] No-slip boundary conditions are employed at the walls and periodic boundary conditions are used in the x and z directions. Aliasing errors from the Fourier transforms are removed using the 3/2-rule detailed in Zang and Hussaini.[52] A zero pressure gradient is imposed in all simulations. Table I provides the dimensions of the computational box, the number of grid points, and the number of spectral modes for the DNS and RNL simulations. The DNS and RNL simulations are initialized with a laminar flow. Turbulence is then initiated by applying the respective stochastic excitations ϵ in (1) and $\mathbf{e}$ in (2) over the time interval $t \in [0, 500]$. These divergence free stochastic excitations are delta correlated in time and delta correlated in space at the level of the spatial Fourier discretization. In order to perform the RNL computations, the DNS code was restricted to the dynamics of (2).

We also perform a number of flow simulations where the flow dynamics of the RNL model is restricted to a single streamwise varying perturbation and the streamwise averaged mean flow. We

TABLE I. Geometry for the numerical simulations. x/δ, y/δ, and z/δ define the computational domain, non-dimensionalized by the channel half-height, δ. N_x, N_y, and N_z are the number of grid points in their respective directions. M_x and M_z are the number of Fourier modes used before dealiasing and M_y is the number of Chebyshev modes used in each simulation.

Case	x/δ	y/δ	z/δ	$N_x \times N_y \times N_z$	$M_x \times M_y \times M_z$
DNS-A	$[0,\ 4\pi]$	$[-1, 1]$	$[0, 4\pi]$	$128 \times 65 \times 128$	$128 \times 65 \times 65$
DNS-B	$[0,\ 8\pi]$	$[-1, 1]$	$[0, 4\pi]$	$128 \times 65 \times 128$	$128 \times 65 \times 65$
DNS-C	$[0,\ 12\pi]$	$[-1, 1]$	$[0, 4\pi]$	$128 \times 65 \times 128$	$128 \times 65 \times 65$
DNS-D	$[0,\ 16\pi]$	$[-1, 1]$	$[0, 4\pi]$	$128 \times 65 \times 128$	$128 \times 65 \times 65$
RNL-A	$[0,\ 4\pi]$	$[-1, 1]$	$[0, 4\pi]$	$16 \times 65 \times 128$	$16 \times 65 \times 65$
RNL-B	$[0,\ 8\pi]$	$[-1, 1]$	$[0, 4\pi]$	$32 \times 65 \times 128$	$32 \times 65 \times 65$
RNL-C	$[0, 12\pi]$	$[-1, 1]$	$[0, 4\pi]$	$48 \times 65 \times 128$	$48 \times 65 \times 65$
RNL-D	$[0, 16\pi]$	$[-1, 1]$	$[0, 4\pi]$	$64 \times 65 \times 128$	$64 \times 65 \times 65$
RNL-E	$[0, 24\pi]$	$[-1, 1]$	$[0, 4\pi]$	$96 \times 65 \times 128$	$96 \times 65 \times 65$
RNL-F	$[0, 32\pi]$	$[-1, 1]$	$[0, 4\pi]$	$96 \times 65 \times 128$	$96 \times 65 \times 65$
RNL-G	$[0, 48\pi]$	$[-1, 1]$	$[0, 4\pi]$	$96 \times 65 \times 128$	$96 \times 65 \times 65$
RNL-H	$[0, 64\pi]$	$[-1, 1]$	$[0, 4\pi]$	$120 \times 65 \times 128$	$120 \times 65 \times 128$
RNL-I	$[0, 72\pi]$	$[-1, 1]$	$[0, 4\pi]$	$138 \times 65 \times 128$	$138 \times 65 \times 65$

implement this restriction by adding a damping term $\xi\mathbf{u}$ to perturbation dynamics (2b) to obtain

$$\mathbf{U}_t + \mathbf{U}\cdot\nabla\mathbf{U} + \nabla P - \frac{1}{R}\Delta\mathbf{U} = -\langle\mathbf{u}\cdot\nabla\mathbf{u}\rangle, \tag{3a}$$

$$\mathbf{u}_t + \mathbf{U}\cdot\nabla\mathbf{u} + \mathbf{u}\cdot\nabla\mathbf{U} + \nabla p - \frac{1}{R}\Delta\mathbf{u} - \xi\mathbf{u} = \mathbf{e}, \tag{3b}$$

$$\nabla\cdot\mathbf{U} = 0, \quad \nabla\cdot\mathbf{u} = 0. \tag{3c}$$

We then restrict the RNL dynamics to a single nonzero Fourier number, $k_x = \pm i$ by increasing the damping coefficient, ξ in (3b), from 0 to $1/\Delta t$ over a period of 100 time steps for all $k_x \neq \pm i$. We refer to these restricted dynamics as the truncated RNL system. The flow geometries and wavelengths associated with the active Fourier number $k_x = \pm i$ for simulations of these restricted RNL systems are given in Table II.

IV. RESULTS

In this section, we first demonstrate the agreement of RNL simulations with DNS in different channel configurations. We then show that turbulence in this RNL system is naturally supported by a small number of streamwise varying modes. In addition, the system can be truncated so that it is supported by a single streamwise varying mode interacting with the mean flow. All simulations in this section are at $R = 1000$; the full parameter set for each simulation is given in Tables I and II.

A. The streamwise wavenumber support of RNL turbulence

The RNL system has been shown to maintain turbulence with a mean flow and structural features that closely resemble those of DNS.[36,37,45] In the current work, we study the RNL system described by (2) across a range of channel configurations. Figure 1 demonstrates that RNL simulations produce mean velocity profiles consistent with those from DNS in channels with streamwise extents varying from $4\pi\delta$ to $16\pi\delta$. Based on the results shown in Figure 1 and observations that the flow structures are consistent with those reported in Ref. 36, we conclude that the RNL system captures the essential features of turbulent flow over a range of operating conditions. In addition, we observe that varying the channel length does not significantly affect the nature of turbulence sustained in the RNL system. We now show that RNL turbulence is naturally supported by a greatly reduced set of streamwise varying wavenumbers. In particular, we demonstrate that when **e** in Equation (2b) is set to 0, the RNL model reduces to a minimal configuration in which only

TABLE II. Geometry for the numerical simulations of the truncated RNL system. λ_d is the wavelength of the undamped streamwise varying perturbations. x/δ, y/δ, and z/δ define the computational domain, non-dimensionalized by the channel half-height, δ. N_x, N_y, and N_z are the number of grid points in their respective directions. M_x and M_z are the number of Fourier modes used before dealiasing and M_y is the number of Chebyshev modes used in each simulation.

Case	λ_d	x/δ	y/δ	z/δ	$N_x \times N_y \times N_z$	$M_x \times M_y \times M_z$
D1	$4\pi\delta$	$[0, 4\pi]$	$[-1, 1]$	$[0, 4\pi]$	$32 \times 65 \times 128$	$32 \times 65 \times 65$
D2	$2\pi\delta$	$[0, 4\pi]$	$[-1, 1]$	$[0, 4\pi]$	$32 \times 65 \times 128$	$32 \times 65 \times 65$
D3	$4\pi\delta/3$	$[0, 4\pi]$	$[-1, 1]$	$[0, 4\pi]$	$32 \times 65 \times 128$	$32 \times 65 \times 65$
D4	$\pi\delta$	$[0, 4\pi]$	$[-1, 1]$	$[0, 4\pi]$	$32 \times 65 \times 128$	$32 \times 65 \times 65$
D5	$4\pi\delta/5$	$[0, 4\pi]$	$[-1, 1]$	$[0, 4\pi]$	$32 \times 65 \times 128$	$32 \times 65 \times 65$
D6	$2\pi\delta/3$	$[0, 4\pi]$	$[-1, 1]$	$[0, 4\pi]$	$32 \times 65 \times 128$	$32 \times 65 \times 65$
D7	$4\pi\delta/7$	$[0, 4\pi]$	$[-1, 1]$	$[0, 4\pi]$	$32 \times 65 \times 128$	$32 \times 65 \times 65$
K1	$48\pi\delta$	$[0, 48\pi]$	$[-1, 1]$	$[0, 4\pi]$	$96 \times 65 \times 128$	$96 \times 65 \times 65$
K2	$24\pi\delta$	$[0, 48\pi]$	$[-1, 1]$	$[0, 4\pi]$	$96 \times 65 \times 128$	$96 \times 65 \times 65$
K3	$16\pi\delta$	$[0, 48\pi]$	$[-1, 1]$	$[0, 4\pi]$	$96 \times 65 \times 128$	$96 \times 65 \times 65$
K4	$12\pi\delta$	$[0, 48\pi]$	$[-1, 1]$	$[0, 4\pi]$	$96 \times 65 \times 128$	$96 \times 65 \times 65$
K5	$48\pi\delta/5$	$[0, 48\pi]$	$[-1, 1]$	$[0, 4\pi]$	$96 \times 65 \times 128$	$96 \times 65 \times 65$
K12	$4\pi\delta$	$[0, 48\pi]$	$[-1, 1]$	$[0, 4\pi]$	$96 \times 65 \times 128$	$96 \times 65 \times 65$
K15	$16\pi\delta/5$	$[0, 48\pi]$	$[-1, 1]$	$[0, 4\pi]$	$96 \times 65 \times 128$	$96 \times 65 \times 65$
K16	$3\pi\delta$	$[0, 48\pi]$	$[-1, 1]$	$[0, 4\pi]$	$96 \times 65 \times 128$	$96 \times 65 \times 65$
K20	$12\pi\delta/5$	$[0, 48\pi]$	$[-1, 1]$	$[0, 4\pi]$	$96 \times 65 \times 128$	$96 \times 65 \times 65$
K24	$2\pi\delta$	$[0, 48\pi]$	$[-1, 1]$	$[0, 4\pi]$	$96 \times 65 \times 128$	$96 \times 65 \times 65$
K25	$48\pi\delta/25$	$[0, 48\pi]$	$[-1, 1]$	$[0, 4\pi]$	$96 \times 65 \times 128$	$96 \times 65 \times 65$
K30	$8\pi\delta/5$	$[0, 48\pi]$	$[-1, 1]$	$[0, 4\pi]$	$96 \times 65 \times 128$	$96 \times 65 \times 65$
K40	$6\pi\delta/5$	$[0, 48\pi]$	$[-1, 1]$	$[0, 4\pi]$	$128 \times 65 \times 128$	$128 \times 65 \times 65$
K50	$24\pi\delta/25$	$[0, 48\pi]$	$[-1, 1]$	$[0, 4\pi]$	$160 \times 65 \times 128$	$128 \times 65 \times 65$
K60	$4\pi\delta/5$	$[0, 48\pi]$	$[-1, 1]$	$[0, 4\pi]$	$160 \times 65 \times 128$	$128 \times 65 \times 65$

a finite number of streamwise varying perturbations are maintained, while the energy in the other streamwise varying perturbations decays exponentially. In order to quantify the energy in the perturbations at each wavenumber k_n, we define the streamwise energy density as the perturbation energy associated with streamwise wavelength λ_n, which is given by

$$E_{\lambda_n}(t) = \int_0^{L_z} \int_{-\delta}^{\delta} \int_0^{L_x} \frac{1}{2} \mathbf{u}_{\lambda_n}(x, y, z, t)^2 \, dx \, dy \, dz. \tag{4}$$

Here, $\mathbf{u}_{\lambda_n}$ is the perturbation, $\mathbf{u} = (u, v, w)$, associated with Fourier components with streamwise wavelength λ_n. The natural support of the RNL turbulence is then defined as the set of streamwise

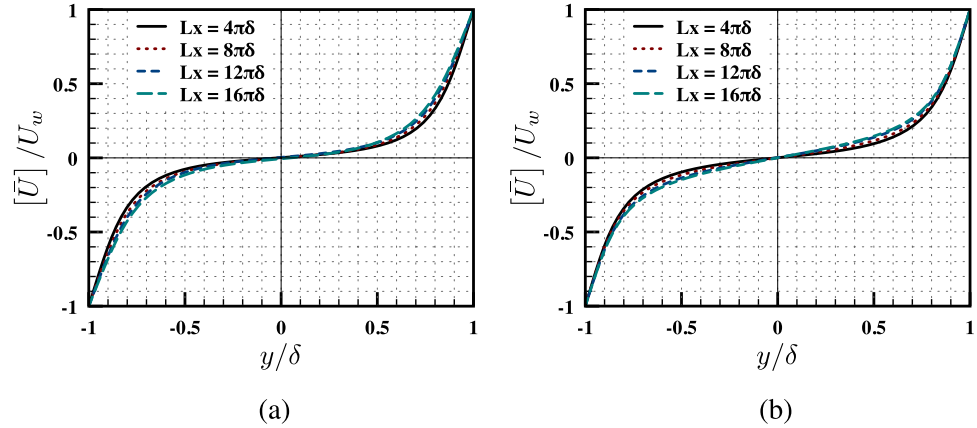

FIG. 1. Turbulent mean velocity profiles (based on a streamwise, spanwise, and time average) from (a) simulations of the RNL model and (b) DNS for channels with $L_x = \{4\pi, 8\pi, 12\pi, 16\pi\}\delta$.

modes n for which

$$\lim_{t\to\infty} E_{\lambda_n}(t) \geq eps, \tag{5}$$

when $\mathbf{e} = 0$ in Equation (2b), where eps is a threshold defined based on the numerical accuracy of the simulation.

Figure 2 demonstrates how the natural support of the RNL system compares to the full streamwise energy spectrum supporting turbulence in DNS. Figures 2(a) and 2(b) show the time evolution of the streamwise energy densities, E_{λ_n}, for cases RNL-D and DNS-D, respectively. Both of these simulations were initiated with a stochastic excitation, respectively, ϵ in (1b) and $\mathbf{e}$ in (2b), containing a full range of streamwise and spanwise Fourier components. The excitation was terminated at $t = 500$. Figure 2(b) demonstrates that in the DNS, all streamwise perturbations remain supported. In contrast, the number of streamwise Fourier components supporting RNL turbulence rapidly converges to the small set comprising its natural support. For the RNL simulation in a $16\pi\delta$ channel, the energy densities associated with all streamwise wavelengths $\lambda_x \leq 8\pi\delta/3$ decay rapidly after the stochastic excitation is removed. This convergence of the RNL natural streamwise Fourier support to a small set of wavenumbers persists over a large range of Reynolds numbers. These results demonstrate that simulations using the RNL system require substantially less computational resources than DNS.

The difference between the unforced RNL system and the NS equations is the removal of the perturbation-perturbation nonlinearity term, $\mathbf{u}\cdot\nabla\mathbf{u} - \langle\mathbf{u}\cdot\nabla\mathbf{u}\rangle$. The maintenance of RNL turbulence supported by a small subset of the streamwise Fourier components demonstrates the existence of a set of active perturbations that are maintained though interactions with the time-dependent streamwise averaged mean flow. The perturbations that naturally decay in the unforced RNL system cannot be sustained without excitation from nonlinear perturbation-perturbation interactions. The fact that the absence of these weakly interacting perturbations does not significantly alter either the mean flow or the maintenance of turbulence suggests that these perturbations do not play a significant role either in the maintenance or regulation of the RNL turbulent state and are in this sense inactive. Previous work demonstrating the close correspondence in the mean profile and the time-averaged Reynolds stress components shown in Figures 1 and 6 in the work of Thomas *et al*.[36] underscores this point. In what follows, we will further characterize the support of turbulence in the RNL system by examining the streamwise energy density as a function of the streamwise extent of the channel.

The natural support of RNL turbulence in a channel with a streamwise extent of $16\pi\delta$ consists of all of the streamwise varying modes with wavelengths longer than $8\pi\delta/3$. This lower limit was

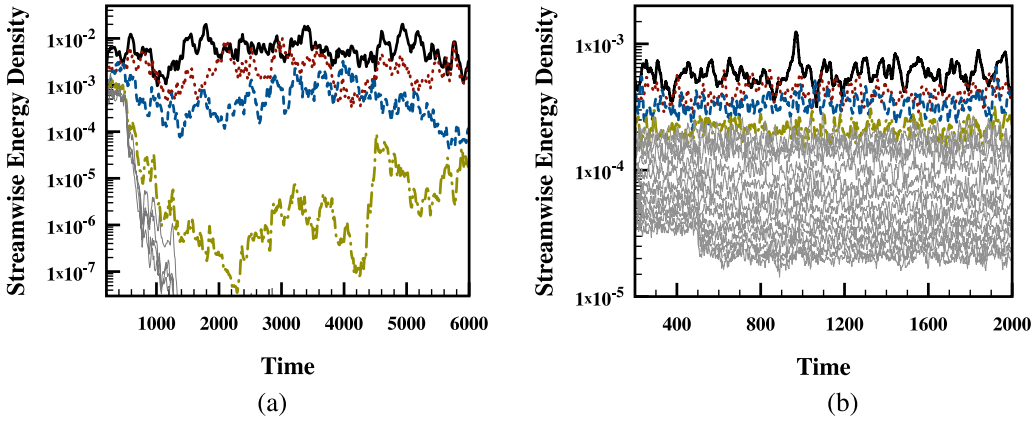

FIG. 2. Selected streamwise energy densities for cases (a) RNL-D and (b) DNS-D at $R = 1000$ for a channel with $L_x = 16\pi\delta$. The energy densities of the streamwise varying perturbations that are supported in the RNL simulation are shown in the following manner: $\lambda_1 = 16\pi\delta$ (black solid), $\lambda_2 = 8\pi\delta$ (red dot), $\lambda_3 = 16\pi\delta/3$ (blue dash), $\lambda_6 = 8\pi\delta/3$ (gold dot-dash). The modes that decay when the RNL is in a self-sustaining state are shown in thin grey lines in both panels.

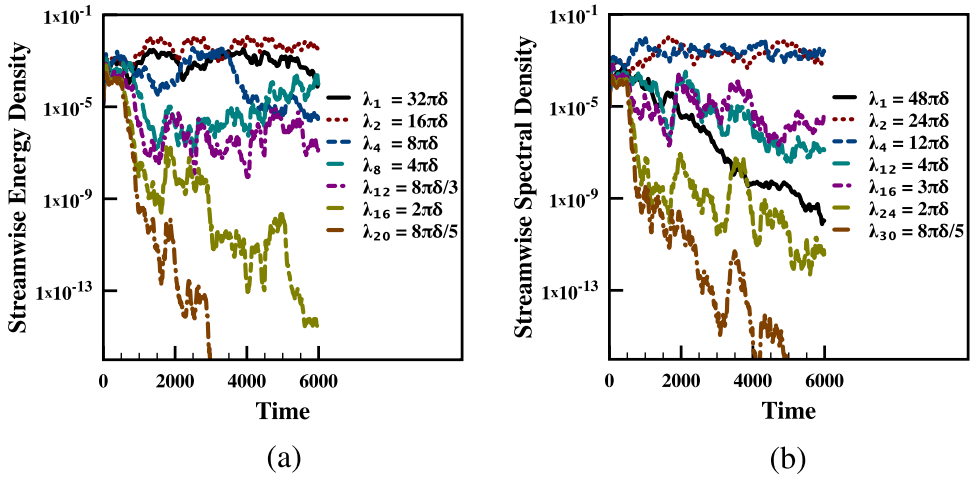

FIG. 3. Streamwise energy densities for (a) case RNL-F and (b) case RNL-G in Table I at $R = 1000$ with streamwise channel lengths $L_x = 32\pi\delta$ and $L_x = 48\pi\delta$, respectively.

previously observed to be $4\pi\delta/3$ for case RNL-A. Each of the RNL simulations described in Table I demonstrates a similar lower limit on the wavelengths included in their natural support. Based on the plot in Figure 2(a), it remains unclear whether there is an upper bound on the wavelengths comprising the natural support of RNL turbulence. In order to investigate this question further, we next consider the unforced RNL model in longer channels.

Figures 3(a) and 3(b), respectively, show the time evolution of the streamwise energy densities, E_{λ_n}, for cases RNL-F and RNL-G with respective streamwise channel lengths $L_x = 32\pi\delta$ and $L_x = 48\pi\delta$. In both of these simulations, turbulence is initiated by applying a stochastic excitation $\mathbf{e}$ in Equation (2b) from $t = 0$ to $t = 500$. Figure 3(a) reveals that in the channel with $L_x = 32\pi\delta$ the streamwise energy density E_{λ_1} is consistently lower than E_{λ_2}. It should be noted that this is the first channel length in this study where this behavior is observed, i.e., in cases RNL-A, RNL-B, RNL-C, and RNL-D, which are described in Table I, the energy density associated with λ_1 has the greatest magnitude. Figure 3(b) shows that for case RNL-G, the streamwise varying mode with the longest wavelength, $\lambda_1 = 48\pi\delta$, clearly decays to zero, confirming the existence of an upper wavelength limit of the natural support of RNL turbulence. The maximum wavelengths in the natural support of RNL turbulence in channels with streamwise extents of $L_x = 48\pi\delta$ and $L_x = 64\pi\delta$ are $\lambda = 24\pi\delta$ and $\lambda = 32\pi\delta$, respectively. From the data across a number of channel configurations, we estimate that the respective lower and upper bounds of the wavelengths corresponding to the set of modes in the natural support of RNL turbulence at $R = 1000$ are approximately $2\pi\delta$ and $32\pi\delta$.

Figure 4 shows the wavelength, λ, at which the largest time-averaged streamwise energy density occurs for each of the cases described in Table II. For RNL simulations with $L_x < 32\pi\delta$ the longest wavelength has the highest mean energy density. However, for the RNL simulations in channels with $L_x \geq 32\pi\delta$, the most energetic wavelength is near $16\pi\delta$. The most prominent exception is case RNL-H where $L_x = 64\pi\delta$. In this case the energy density for $\lambda_6 = 32\pi\delta/3$ is 1.7% greater than the energy density associated with $\lambda_4 = 16\pi\delta$. We also note that cases RNL-E and RNL-G with respective channel lengths of $24\pi\delta$ and $72\pi\delta$ do not admit a streamwise mode with a wavelength of $16\pi\delta$. In case RNL-E the two nearest wavelengths $24\pi\delta$ and $12\pi\delta$ have nearly identical energy densities, and for case RNF-G the maximum energy density occurs at $\lambda_4 = 18\pi\delta$. We conclude that $16\pi\delta$ is a reasonable approximation for the ideal length for structures interacting with the mean flow regardless of the channel length.

Figure 4 also shows the long and short wavelength limits, respectively, denoted by λ_{max} and λ_{min}, corresponding to the highest and lowest wavenumbers of the modes in the natural support of the RNL system at $R = 1000$. The short wavelength limit shows relative invariance with respect to the streamwise extent of the channel, L_x. For cases with $L_x \in [16\pi, 96\pi]\delta$, the short wavelength limit is constrained to a small range of values $\lambda_{min} \in [5\pi/2, 3\pi]\delta$, whereas cases with $L_x < 16\pi\delta$

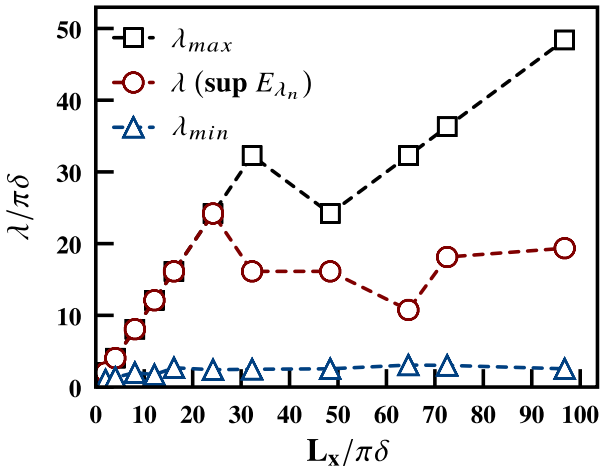

FIG. 4. The wavelengths corresponding to the longest λ_{max} (black squares) and shortest λ_{min} (blue triangles) modes in the natural support of the RNL system along with the wavelength corresponding to the mode with the largest average energy density, $\lambda(\sup E_{\lambda_n})$ (red circles) all as a function of streamwise channel length, L_x, for $R = 1000$. Lines are shown solely to guide the eye.

have smaller λ_{min} values. We do not see the same invariance in the long wavelength limit of this support. For simulations with $L_x \in [2\pi, 24\pi]\delta$, the long wavelength limit, λ_{max}, corresponds to λ_1, the wavelength associated with the channel length. For channels with $L_x \in [32\pi, 96\pi]\delta$ the long wavelength limit, λ_{max}, corresponds to λ_2, the wavelength associated with the channel half-length. In describing the long wavelength limit, we are limited by the discretization in the streamwise direction. If there is an invariant for the long wavelength limit, it could only be discovered by examining cases with extremely large streamwise channel lengths, which is a direction for future work. For simulations in channels with $L_x \in [2\pi, 16\pi]\delta$, the largest time-averaged streamwise energy density, $\lambda(\sup E_{\lambda_n})$, also occurs at wavelengths associated with the channel length, λ_1. For systems with $L_x \in [24\pi, 96\pi]\delta$, this maximum generally occurs at $\lambda = 16\pi\delta$ unless the streamwise discretization does not permit this wavelength. In those cases, $\lambda(\sup E_{\lambda_n})$ occurs at the permitted wavelength that is closest to $16\pi\delta$, i.e., for $L_x = 72\pi\delta$, the maximum time-averaged streamwise energy density occurs at $\lambda_4 = 18\pi\delta$.

B. Truncating the streamwise Fourier support of the RNL system

The results in Sec. IV A illustrate the natural support of RNL turbulence under a number of different conditions. We now show that RNL turbulence can be supported even in cases where the dynamics is restricted to a single streamwise varying perturbation interacting with the streamwise averaged mean flow. We then explore the relationship between the natural support of the RNL system and that of the truncated RNL system. In what follows, we refer to the RNL system with no streamwise Fourier mode truncation as the baseline RNL system. In Section IV A, we observed that simulations of case RNL-G exhibit both the upper and lower limits of the natural support of RNL turbulence, so we study the truncated systems in channels with $L_x = 48\pi\delta$. The numerical details for the truncated RNL simulations are provided in Section III and a full list of the simulation parameters for these cases is given in Table II.

Figure 5 demonstrates that truncated RNL systems all have an appropriately shaped mean velocity profile (based on a streamwise, spanwise, and time average) and that these profiles are qualitatively similar to those obtained with the baseline RNL system. In particular, for cases K3 and K4, the profiles are almost identical and have R_τ values of 53.4 and 57.0, respectively, which are close to the value of $R_\tau = 56$ in the baseline system. Cases K12, K16, K24, and K40 show higher shear stress at the wall and correspondingly higher R_τ values of 64.5, 69.6, and 64.5, respectively. Selective filtering of streamwise varying perturbations in the RNL system was previously shown to strongly influence both the mean velocity profile and the spanwise spectra of the velocity field.[53]

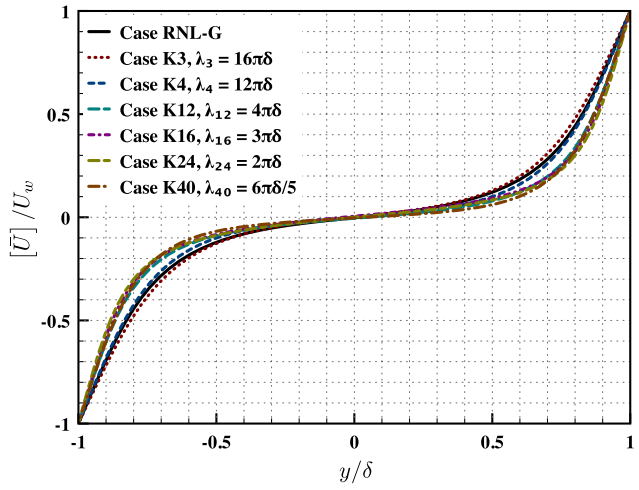

FIG. 5. Turbulent mean velocity profiles (based on a streamwise, spanwise, and time average) obtained for cases RNL-G, K3, K4, K12, K16, K24, and K40 all at $R = 1000$. Cases where the RNL is truncated to longer wavelengths exhibit a mean profile similar to the baseline RNL simulation (case RNL-G).

Previous work has also shown that higher dissipation is associated with the inclusion of shorter wavelength perturbations.[36] This implies that the higher wavenumber and therefore higher dissipation cases K12, K16, K24, and K40 require a higher shear stress in order to attain a statistical equilibrium, which is the trend observed in the mean velocity profiles of Figure 5.

Figures 6(a) and 6(b) respectively show the time evolution of $\sqrt{2E_{\lambda_n}}$ for simulations of case K3 and case K4, in Table II. The wavelengths of the untruncated modes, respectively, $\lambda_3 = 16\pi\delta$

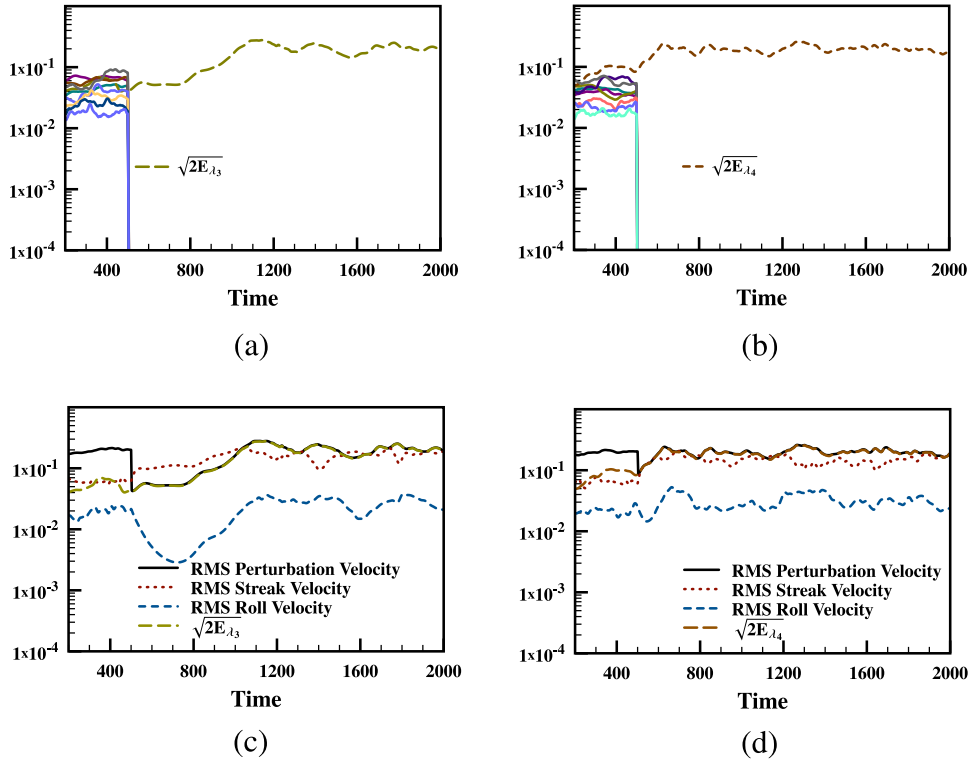

FIG. 6. Panels (a) and (b) show $\sqrt{2E_{\lambda_n}}$ versus time for cases K3 and K4, respectively. Panels (c) and (d) show $\sqrt{2E_{\lambda_n}}$ for the undamped wavelength ($\lambda_3 = 16\pi\delta$ and $\lambda_4 = 12\pi\delta$, respectively), the RMS perturbation velocity, U_{Pert}, the RMS streak velocity, U_{Streak}, and the RMS roll velocity, U_{Roll}, for cases K3 and K4, respectively. In all panels, $R = 1000$.

and $\lambda_4 = 12\pi\delta$, are both within the natural support of the RNL model in a channel with $L_x = 48\pi\delta$, as shown in Figures 3(b) and 4. Both of these cases exhibit self-sustaining turbulent behavior despite the severe restriction in the streamwise harmonics. The rapid decay of the truncated wavenumbers subsequent to the removal of the stochastic excitation at $t = 500$ is evident in Figures 6(a) and 6(b).

Figures 6(c) and 6(d), respectively, replot $\sqrt{2E_{\lambda_n}}$ in Figures 6(a) and 6(b) alongside the RMS perturbation velocity,

$$U_{Pert} \coloneqq \sqrt{\sum_n 2E_{\lambda_n}}, \tag{6}$$

the RMS streak velocity,

$$U_{Streak} \coloneqq \sqrt{\int_0^{L_z}\int_{-\delta}^{\delta} (U - [U])^2 \, dy \, dz}, \tag{7}$$

and the RMS roll velocity,

$$U_{Roll} \coloneqq \sqrt{\int_0^{L_z}\int_{-\delta}^{\delta} V^2 + W^2 \, dy \, dz}. \tag{8}$$

We note that in simulations for cases K3 and K4, both the RMS perturbation velocity, U_{Pert}, and the RMS roll velocity, U_{Roll}, return to levels comparable to those prior to the truncation, after a transient period. From Figures 6(c) and 6(d), it is clear that this adjustment occurs over a much longer time interval for case K3 as compared to case K4.

Figure 7 shows the same results as in Figure 6 for case K24. The single undamped streamwise varying perturbation wavelength of $\lambda_{24} = 2\pi\delta$ corresponds to a mode that is well outside of the natural support of the associated RNL-G (baseline) case; however, this system is still able to sustain RNL turbulence with a reasonable mean profile as seen in Figure 5. For this case, $\sqrt{2E_{\lambda_{24}}}$ is approximately 5% of the RMS perturbation velocity of the flow. When the damping is applied at $t = 500$, the value of $\sqrt{2E_{\lambda_{24}}}$ increases by an order of magnitude such that $\sqrt{2E_{\lambda_{24}}}$ is nearly the same as the time-averaged RMS perturbation velocity prior to the application of the damping.

Figure 8(a) shows the streamwise energy densities for case K2 in which only $\lambda_2 = 24\pi\delta$ and the mean flow is retained. In this case, the flow becomes laminar after the damping is introduced and this behavior leads us to conclude that the RNL system in a $48\pi\delta$ channel cannot sustain turbulence when the dynamics is restricted to perturbation structures of length $\lambda_2 = 24\pi\delta$ interacting with the mean flow. The RNL system also cannot sustain turbulence for case K1 in which only $\lambda_1 = 48\pi\delta$ is retained.

As in the natural support of the baseline RNL system, there is a high wavenumber mode that corresponds to a short wavelength limit beyond which turbulence is not robustly maintained. This

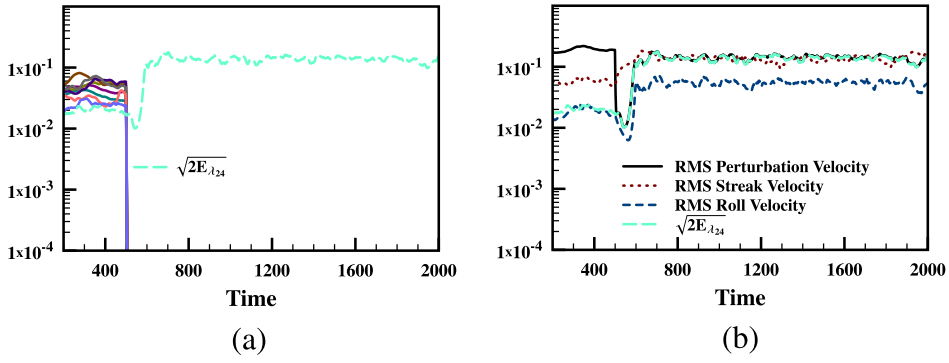

FIG. 7. (a) $\sqrt{2E_{\lambda_n}}$ versus time for case K24. (b) $\sqrt{2E_{\lambda_n}}$ for the undamped wavelength (λ_{24}), the RMS perturbation velocity, U_{Pert}, the RMS streak velocity, U_{Streak}, and the RMS roll velocity, U_{Roll}, for case K24. In all panels, $R = 1000$.

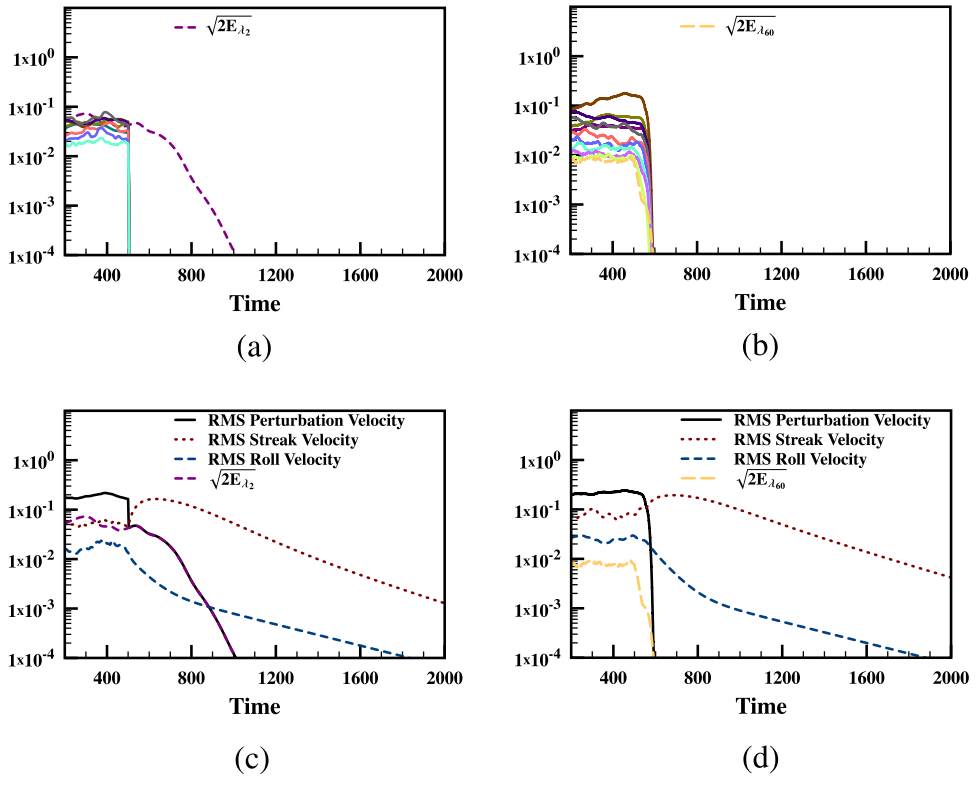

FIG. 8. Panels (a) and (b) show $\sqrt{2E_{\lambda_n}}$ versus time resulting for cases K2 and K60, respectively. Panels (c) and (d) show $\sqrt{2E_{\lambda_n}}$ for the undamped wavelengths (λ_2 and λ_{60}, respectively), the RMS perturbation velocity, U_{Pert}, the RMS streak velocity, U_{Streak}, and the RMS roll velocity, U_{Roll}, for cases K2 and K60, respectively. In all panels, $R = 1000$.

behavior can be seen in Figures 8(b) and 8(d), which reveals the existence of a short wavelength limit beyond which RNL turbulence can be supported by perturbations at a single streamwise varying wavenumber. As in the case of the long wavelength boundary, the undamped wavelength, in this case λ_{60}, does not show any increase in energy. There is a region of uncertainty concerning the maintenance of RNL turbulence in cases where a relatively short wavelength is retained. For the conditions used in K50, K60, and K70, some cases maintained turbulence, while others relaminarized. Similarly some of the simulations with the conditions of case D6, which corresponds to a truncated RNL simulation retaining only $\lambda_6 = 2\pi\delta/3$, maintain turbulence and others relaminarize. However, in case D7 which retains only the mode associated with $\lambda_7 = 4\pi\delta/7$, the simulation always relaminarizes. This conditional relaminarization behavior in the truncated RNL system may be related to the state of the system at the initiation of damping. However, fully characterizing the factors that lead to the sustenance of turbulence versus relaminarization given a particular sequence of random forcings to initiate turbulence is a topic of ongoing work.

The natural support of RNL turbulence and the single streamwise varying modes that support turbulence in the truncated RNL system for channels with $L_x = 48\pi\delta$ is summarized in Figure 9. The wavelengths associated with the natural support of baseline RNL system are shaded grey. The modes in the natural support for the baseline RNL systems correspond to wavelengths ranging from approximately $2\pi\delta$ to $24\pi\delta$. In contrast, the long wavelength limit associated with the truncated RNL system is approximately $16\pi\delta$. The short wavelength limit is approximately $\pi\delta$, which is also shorter than the lowest mode in the natural support of the baseline RNL model. A full characterization of the factors determining the bounds of both the set comprising the streamwise Fourier support of the baseline RNL model and the set of single streamwise varying modes that can maintain turbulence through interactions with the mean flow will provide further insight into the nature of the RNL SSP and are the subject of ongoing work.

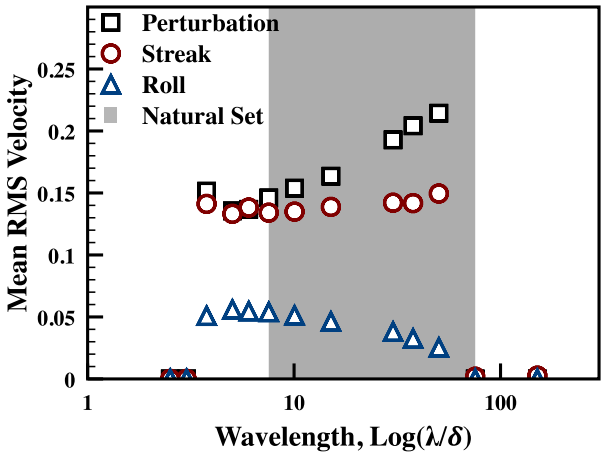

FIG. 9. Time-averaged RMS perturbation velocity, U_{Pert} (black squares), RMS streak velocity, U_{Streak} (red circles), and RMS roll velocity, U_{Roll} (blue triangles) for the set of truncated RNL systems in Table II with $L_x = 48\pi\delta$. All simulations are at $R = 1000$. The shaded region indicates the natural streamwise Fourier support of the baseline RNL model. The set of perturbation wavelengths that sustain turbulence in the truncated RNL system is disjoint from the natural support of the RNL dynamics.

Figure 9 also demonstrates the impact of truncation on the RMS velocities associated with the perturbation energy and important flow structures. The RMS roll velocity, U_{Roll}, increases with decreasing truncation wavelength, plateauing near the point where the truncation can no longer sustain turbulence. Conversely, the RMS perturbation velocity, U_{Pert}, decreases along with the truncation wavelength. This increase in RMS perturbation velocity with truncation wavelength is also associated with an increase in the intensity of the streamwise normal Reynolds stress component. There is no clear trend in the RMS streak velocity. We conclude that the choice of truncation wavelength strongly influences the coupling between the perturbations and the roll circulation, while the streak amplitude is relatively robust to truncation. Understanding how truncation affects a wider range of flow properties is the subject of ongoing work.

V. CONCLUSIONS AND DIRECTIONS FOR FUTURE WORK

In this paper, we have shown that the RNL system intrinsically produces a minimal representation of turbulence that is supported by a streamwise averaged mean flow and a small set of streamwise varying perturbations. This minimal state arises spontaneously when the stochastic parametrization of the nonlinear interactions among the streamwise varying perturbations is eliminated in the perturbation equation. The retained modes actively participate in the transfer of energy from the time-dependent streamwise averaged mean flow to the perturbation field and we refer to this set of modes as the natural support of self-sustaining turbulence in the RNL system. Convergence of the support of RNL turbulence to this reduced set of streamwise harmonics is consistent with the results reported in Ref. 45. That work demonstrated that the RNL perturbation dynamics with no external excitation is a time-dependent linear system that will eventually attain the asymptotic perturbation structure spanned by its top Lyapunov vectors.

The results also demonstrate that the ability of the RNL system to self-sustain turbulence is remarkably robust. In particular, we show that RNL turbulence can be sustained when the dynamics is limited to comprise a single streamwise varying mode interacting with the streamwise averaged mean flow. The wavelengths of the streamwise varying perturbations that comprise the natural support of the RNL turbulence lie in a closed interval and our calculations suggest that this interval becomes independent of channel size for long enough channels. The set of single streamwise wavenumbers that support RNL turbulence is found to extend to shorter wavelengths than those that are present in the natural support of the baseline RNL model but not to longer ones.

The results presented here and the previously reported close correspondence between RNL simulations and DNS suggest that the fundamental mechanisms underlying wall-turbulence can be analyzed using highly simplified RNL systems. The RNL framework provides distinct advantages over other minimal models that have been employed. First, the equations are directly derived from the NS equations and are easy to implement within an existing DNS code. Second, implementations of RNL minimal models do not rely on a particular Reynolds number or channel size and therefore, Reynolds number trends as well as the dynamics of the RNL SSP in large channels can be explored using these models. Finally, the RNL system inherently captures the dynamics of key flow structures as intrinsic elements of the system dynamics in a computationally and an analytically tractable framework. These advantages make it a powerful tool for probing the dynamics of wall-turbulence. The insight gained through such studies can then be tested using DNS and exploited to develop flow control strategies.

ACKNOWLEDGMENTS

The authors would like to thank Binh K. Lieu and Mihailo R. Jovanović for many fruitful discussions, as well as B.K.L.'s contributions to early versions of the simulation codes. Financial support from the NSF through award numbers AGS-1246929 (B.F.F.) and IIA-1243482 (V.L.T. and D.F.G) is gratefully acknowledged.

[1] J. L. Lumley, "The structure of inhomogeneous turbulence," in *Atmospheric Turbulence and Radio Wave Propagation*, edited by A. M. Yaglom and V. I. Tatarskii (Nauka, Moscow, 1967), pp. 166–178.
[2] T. R. Smith, J. Moehlis, and P. Holmes, "Low-dimensional modelling of turbulence using the proper orthogonal decomposition: A tutorial," Nonlinear Dyn. **41**, 275–307 (2005).
[3] B. F. Farrell and P. J. Ioannou, "Accurate low-dimensional approximation of the linear dynamics of fluid flow," J. Atmos. Sci. **58**, 2771–2789 (2001).
[4] C. Rowley, "Model reduction for fluids, using balanced proper orthogonal decomposition," Int. J. Bifurcation Chaos Appl. Sci. Eng. **15**, 997–1013 (2005).
[5] C. Rowley, I. Mezi, S. Bagheri, P. Schlatter, and D. Henningson, "Reduced-order models for flow control: Balanced models and Koopman modes," IUTAM Bookseries **18**, 43–50 (2010).
[6] J. Jiménez and P. Moin, "The minimal flow unit in near-wall turbulence," J. Fluid Mech. **225**, 213–240 (1991).
[7] J. M. Hamilton, J. Kim, and F. Waleffe, "Regeneration mechanisms of near-wall turbulence structures," J. Fluid Mech. **287**, 317–348 (1995).
[8] J. Jiménez, G. Kawahara, M. P. Simens, M. Nagata, and M. Shiba, "Characterization of near-wall turbulence in terms of equilibrium and bursting solutions," Phys. Fluids **17**, 015105 (2005).
[9] G. Kawahara, M. Uhlmann, and L. Van Veen, "The significance of simple invariant solutions in turbulent flows," Annu. Rev. Fluid Mech. **44**, 203–225 (2012).
[10] M. Nagata, "Three-dimensional traveling-wave solutions in plane Couette flow," J. Fluid Mech. **217**, 519–527 (1990).
[11] J. F. Gibson, J. Halcrow, and P. Cvitanović, "Equilibrium and travelling-wave solutions of plane Couette flow," J. Fluid Mech. **638**, 243–266 (2009).
[12] J. Moehlis, H. Faisst, and B. Eckhardt, "A low-dimensional model for turbulent shear flows," New J. Phys. **6**, 56 (2004).
[13] L. Tuckerman and D. Barkley, "Patterns and dynamics in transitional plane Couette flow," Phys. Fluids **23**, 041301 (2011).
[14] B. F. Farrell and P. J. Ioannou, "Generalized stability. Part I: Autonomous operators," J. Atmos. Sci. **53**, 2025–2040 (1996).
[15] B. F. Farrell and P. J. Ioannou, "Generalized stability. Part II: Non-autonomous operators," J. Atmos. Sci. **53**, 2041–2053 (1996).
[16] B. F. Farrell, "Optimal excitation of perturbations in viscous shear flow," Phys. Fluids **31**, 2093–2102 (1988).
[17] L. H. Gustavsson, "Energy growth of three-dimensional disturbances in plane Poiseuille flow," J. Fluid Mech. **224**, 241–260 (1991).
[18] L. N. Trefethen, A. E. Trefethen, S. C. Reddy, and T. A. Driscoll, "Hydrodynamic stability without eigenvalues," Science **261**, 578–584 (1993).
[19] S. C. Reddy and D. S. Henningson, "Energy growth in viscous shear flows," J. Fluid Mech. **252**, 209–238 (1993).
[20] B. F. Farrell and P. J. Ioannou, "Stochastic forcing of the linearized Navier–Stokes equations," Phys. Fluids A **5**, 2600–2609 (1993).
[21] B. Bamieh and M. Dahleh, "Energy amplification in channel flows with stochastic excitation," Phys. Fluids **13**, 3258–3269 (2001).
[22] M. R. Jovanović and B. Bamieh, "Componentwise energy amplification in channel flows," J. Fluid Mech. **534**, 145–183 (2005).
[23] K. M. Butler and B. F. Farrell, "Three-dimensional optimal perturbations in viscous shear flows," Phys. Fluids **4**, 1637–1650 (1992).
[24] D. S. Henningson, "Comment on "Transition in shear flows. Nonlinear normality versus non-normal linearity" [Phys. Fluids 7, 3060 (1995)]," Phys. Fluids **8**, 2257–2258 (1996).
[25] D. S. Henningson and S. C. Reddy, "On the role of linear mechanisms in transition to turbulence," Phys. Fluids **6**, 1396–1398 (1994).

[26] K. M. Butler and B. F. Farrell, "Optimal perturbations and streak spacing in turbulent shear flow," Phys. Fluids A **3**, 774–776 (1993).
[27] J. Kim and J. Lim, "A linear process in wall bounded turbulent shear flows," Phys. Fluids **12**, 1885–1888 (2000).
[28] M. R. Jovanović and B. Bamieh, "Modeling flow statistics using the linearized Navier-Stokes equations," in *Proceedings of the 40th IEEE Conference on Decision and Control (Orlando, FL)* (IEEE, New York, NY, 2001), Vol. 5, pp. 4944–4949.
[29] A. Zare, M. R. Jovanović, and T. T. Georgiou, "Completion of partially known turbulent flow statistics," in *Proceedings of the American Control Conference* (IEEE, Portland, OR, 2014), pp. 1674–1679.
[30] B. F. Farrell and P. J. Ioannou, "Perturbation structure and spectra in turbulent channel flow," Theor. Comput. Fluid Dyn. **11**, 215–227 (1998).
[31] J. C. del Álamo and J. Jiménez, "Linear energy amplification in turbulent channels," J. Fluid Mech. **559**, 205–213 (2006).
[32] Y. Hwang and C. Cossu, "Amplification of coherent structures in the turbulent Couette flow: An input–output analysis at low Reynolds number," J. Fluid Mech. **643**, 333–348 (2010).
[33] C. Cossu, G. Pujals, and S. Depardon, "Optimal transient growth and very large scale structures in turbulent boundary layers," J. Fluid Mech. **619**, 79–94 (2009).
[34] R. Moarref and M. R. Jovanović, "Model-based design of transverse wall oscillations for turbulent drag reduction," J. Fluid Mech. **707**, 205–240 (2012).
[35] B. F. Farrell and P. J. Ioannou, "Structural stability of turbulent jets," J. Atmos. Sci. **60**, 2101–2118 (2003).
[36] V. Thomas, B. K. Lieu, M. R. Jovanović, B. F. Farrell, P. Ioannou, and D. F. Gayme, "Self-sustaining turbulence in a restricted nonlinear model of plane Couette flow," Phys. Fluids **26**, 105112 (2014).
[37] N. C. Constantinou, A. Lozano-Durán, M.-A. Nikolaidis, B. F. Farrell, P. J. Ioannou, and J. Jiménez, "Turbulence in the highly restricted dynamics of a closure at second order: Comparison with DNS," J. Phys.: Conf. Ser. **506**, 1–18 (2014).
[38] J. D. Swearingen and R. F. Blackwelder, "The growth and breakdown of streamwise vortices in the presence of a wall," J. Fluid Mech. **182**, 255–290 (1987).
[39] H. P. Blakewell and L. Lumley, "Viscous sublayer and adjacent wall region in turbulent pipe flow," Phys. Fluids **10**, 1880–1889 (1967).
[40] J. Jiménez, "Near-wall turbulence," Phys. Fluids **25**, 101302 (2013).
[41] W. Schoppa and F. Hussain, "Coherent structure generation in near-wall turbulence," J. Fluid Mech. **453**, 57–108 (2002).
[42] F. Waleffe, "On a self-sustaining process in shear flows," Phys. Fluids A **9**, 883–900 (1997).
[43] P. Hall and S. Sherwin, "Streamwise vortices in shear flows: Harbingers of transition and the skeleton of coherent structures," J. Fluid Mech. **661**, 178–205 (2010).
[44] B. F. Farrell and P. J. Ioannou, "Perturbation growth and structure in time dependent flows," J. Atmos. Sci. **56**, 3622–3639 (1999).
[45] B. F. Farrell and P. J. Ioannou, "Dynamics of streamwise rolls and streaks in turbulent wall-bounded shear flow," J. Fluid Mech. **708**, 149–196 (2012).
[46] U. Frisch, *Turbulence: The Legacy of A. N. Kolmogorov* (Cambridge University Press, 1995).
[47] E. Hopf, "Statistical hydromechanics and functional calculus," J. Ration. Mech. Anal. **1**, 87–123 (1952).
[48] J. F. Gibson, "Channelflow: A spectral Navier–Stokes simulator in C++," Technical Report (U. New Hampshire, 2014) http://www.Channelflow.org.
[49] J. F. Gibson, J. Halcrow, and P. Cvitanović, "Visualizing the geometry of state space in plane Couette flow," J. Fluid Mech. **611**, 107–130 (2008), e-print arXiv:0705.3957.
[50] R. Peyret, *Spectral Methods for Incompressible Flows* (Springer-Verlag, 2002).
[51] C. Canuto, M. Hussaini, A. Quateroni, and T. Zhang, *Spectral Methods in Fluid Dynamics* (Springer-Verlag, 1988).
[52] T. A. Zang and M. Y. Hussaini, "Numerical experiments on subcritical transition mechanism," in *AIAA, Aerospace Sciences Meeting,* 85-0296 (Reno, NV, 1985).
[53] J. U. Bretheim, C. Meneveau, and D. F. Gayme, "Standard logarithmic mean velocity distribution in a band-limited restricted nonlinear model of turbulent flow in a half-channel," Phys. Fluids **27**, 011702 (2015).